

Article

Palustrine Sediments between Two Isolated Shallow Carbonate Platforms (Aptian–Albian Transition, Prebetic of Jaén, South Spain)

Luis M. Nieto ^{*}, José Miguel Molina , Pedro Alejandro Ruiz-Ortiz, José Manuel Castro, Matías Reolid 
and Ginés A. de Gea 

Departamento de Geología and CEACTEMA, Universidad de Jaén, 23071 Jaen, Spain; jmmolina@ujaen.es (J.M.M.); paruiz@ujaen.es (P.A.R.-O.); jmcastro@ujaen.es (J.M.C.); mreolid@ujaen.es (M.R.); gadegea@ujaen.es (G.A.d.G.)

* Correspondence: lmnieto@ujaen.es

Abstract: During the Aptian–Albian transition, an extensional phase of the Central Atlantic which affected the Prebetic carbonate platform (South Iberian Continental Margin, northwestern margin of the Tethys) occurred. A graben morphology was developed in the platform coeval to a relative sea level fall. As a consequence, palustrine facies characterized by rhizoliths and some pond deposits of black lutites were established. Over these palustrine sediments, a second shallow carbonate platform was built during the early Albian. However, this process was not abrupt, as several levels with orbitolines and rudists were deposited intercalated between the continental facies, recording the transition to a new shallow marine carbonate platform developed during the Early Albian. The presence of these continental palustrine sediments between two episodes of shallow carbonate platform is described for the first time in the Prebetic. The demise of an upper Aptian isolated shallow carbonate platform drove to the deposition of these palustrine sediments in an extensional tectonic regime.

Keywords: South Iberian Continental Margin; Prebetic; Aptian–Albian transition; shallow carbonate platform; palustrine facies; charophyte; carbonate platform demise



Citation: Nieto, L.M.; Molina, J.M.; Ruiz-Ortiz, P.A.; Castro, J.M.; Reolid, M.; de Gea, G.A. Palustrine Sediments between Two Isolated Shallow Carbonate Platforms (Aptian–Albian Transition, Prebetic of Jaén, South Spain). *Minerals* **2022**, *12*, 116. <https://doi.org/10.3390/min12020116>

Academic Editor:
Enrique Gomez-Rivas

Received: 12 December 2021

Accepted: 17 January 2022

Published: 20 January 2022

Publisher's Note: MDPI stays neutral with regard to jurisdictional claims in published maps and institutional affiliations.



Copyright: © 2022 by the authors. Licensee MDPI, Basel, Switzerland. This article is an open access article distributed under the terms and conditions of the Creative Commons Attribution (CC BY) license (<https://creativecommons.org/licenses/by/4.0/>).

1. Introduction

The Aptian–Albian transition is an interesting interval at a global scale, which records the occurrence of the Oceanic Anoxic Event 1b, associated to a global perturbation of the carbon cycle and regional deposition of organic-rich deposits, particularly in the western Tethys [1]. In addition, this interval records a remarkable climate change toward more humid and warm conditions after the cooling snap of the late Aptian [2], and a notable biotic turnover in marine faunas [3]. This climate change was concomitant to the opening of gateways in the South Atlantic and Southern Ocean basins [4], leading to changes in the global marine currents. In the Southern Iberian Continental Margin (SICM), this boundary records the end of the urgonian carbonate platforms and the beginning of a mixed carbonate-terrigenous deposition under an increase of the terrestrial runoff. Deposition occurred mostly in highly subsident sectors, whereas wide parts of the margin record a sedimentary hiatus, probably related to a tectonic extensional pulse occurred during this interval [5,6]. This extensional pulse is related to the opening of the Central Atlantic and the development of the Alpine Tethys rift [7], when the connection between the Tethys and the Central and South Atlantic was being generated.

In this time, the Iberian Plate and their margins were located in the boundary between the Tropical–Equatorial hot arid belt and the Northern High-latitude Temperate humid belt [8,9], in a latitude between 20° N and 30° N [1]. A major platform drowning episode is registered in the northern Tethyan margins during the Aptian–Albian transition [10–12]. This event has been related to a eustatic highstand recorded in several transgressive system

tracts [1,11]. As a consequence, low terrigenous input, black shale facies, and marine organic matter were deposited under these relative sea level conditions [1,10,11,13].

In the SICM, the Aptian–Albian transition is represented by the boundary between the sedimentary episodes K4 (Aptian) and K5 (lower–middle Albian) [14]. In the subsiding domain of the Prebetic (Internal Prebetic), the carbonate platform development was widespread, recorded as the Llopis Formation (lower Aptian) and the Seguilí Formation (upper Aptian). In the non-subsiding domain or External Prebetic, only unusual marine carbonate platforms were developed as a consequence of the Cenomanian transgression. The upper boundary of the K4 Episode is an unconformity with a hiatus embracing the latest Aptian and earliest Albian [15,16]. This Aptian–Albian transition in the Prebetic is marked by an extensive discontinuity, although locally, in some subsiding areas of the Prebetic of Alicante and the Prebetic of Jaén, the transition is registered in shallow marine carbonates [5,17] and locally interbedded with freshwater and edaphic deposits. The main features of the K5 Episode are the important lateral facies changes from continental or littoral deposits in the External Prebetic (non-subsiding domain) to mixed platform (Sácaras Formation) and hemipelagic sedimentation with ammonites in the Internal Prebetic [5,6,14,18].

A stratigraphic succession of shallow platform carbonates capped by continental deposits of the Aptian–Albian transition, belonging to the Prebetic of Jaén [19] is analyzed in this research. The Prebetic of Jaén is the westernmost part of the Prebetic platform with Cretaceous sedimentary sequences similar to others outcropping in the Internal Prebetic [20,21]. However, in the Sierra de Bedmar-Jódar, the most remarkable feature of the Aptian–Albian transition deposits is the presence of a continental unit (palustrine sediments with paleosols), not recognized in other successions of the Internal Prebetic. The aim of this research is to analyze the stratigraphy, sedimentology, and paleontology of these rocks and their meaning in the evolution of this area of the SICM.

2. Geological Setting

The Sierra de Bedmar-Jódar belongs to the Prebetic of Jaén [19,21,22], located to the west of the Tíscar fault, an important tectonic lineament that marks the end of the large Prebetic outcrops of the Cazorla, Segura and Las Villas units (Figure 1). The Sierra de Bedmar-Jódar is made up by Cretaceous to Miocene rocks. The structure of these units arranged in an anticline structure tilted to the NW. The southern flank shows a mean dip of 45°, while the northern flank is subvertical or is slightly inverted. The axis of the fold is curved, convex to the NW-W, with an average strike of N30° E. This unit is part of the betic thrust front and is disposed over the Neogene of the Guadalquivir Basin, that was thrust by the subbetic units between the Burdigalian and the Messinian, with tectonic net movement toward the N-NW and W [23].

The Cretaceous is represented by Valanginian–Cenomanian carbonates [21,22]. An unconformity with an Hauterivian–Barremian hiatus has been detected between the Valanginian and the Aptian rocks. The Valanginian sediments (Los Villares Formation) are an alternance of marly limestones and marls, with some sandstone levels, sedimented in hemipelagic environments (Figure 2). The Aptian–Albian carbonates were deposited in shallow-marine environments dominated by lagoon facies [20,24]. The studied Aptian carbonates can be correlated with the Llopis and Seguilí Formations defined in the Prebetic of Alicante [5,6,17,19]. The continental sediments studied are overlying the top of the Seguilí Formation. The Albian carbonates are represented by the Sácaras and Jumilla Formations defined also in the eastern Prebetic outcrops [5,6,17,19] (Figures 1 and 2). The Aptian–Albian carbonate platform cropping-out in the Sierra de Bedmar-Jódar, was developed on a tilted fault block dipping to the NE, as a consequence of the Atlantic rifting stage that affected the SICM at the end of the Early Cretaceous [16,19,21,22].

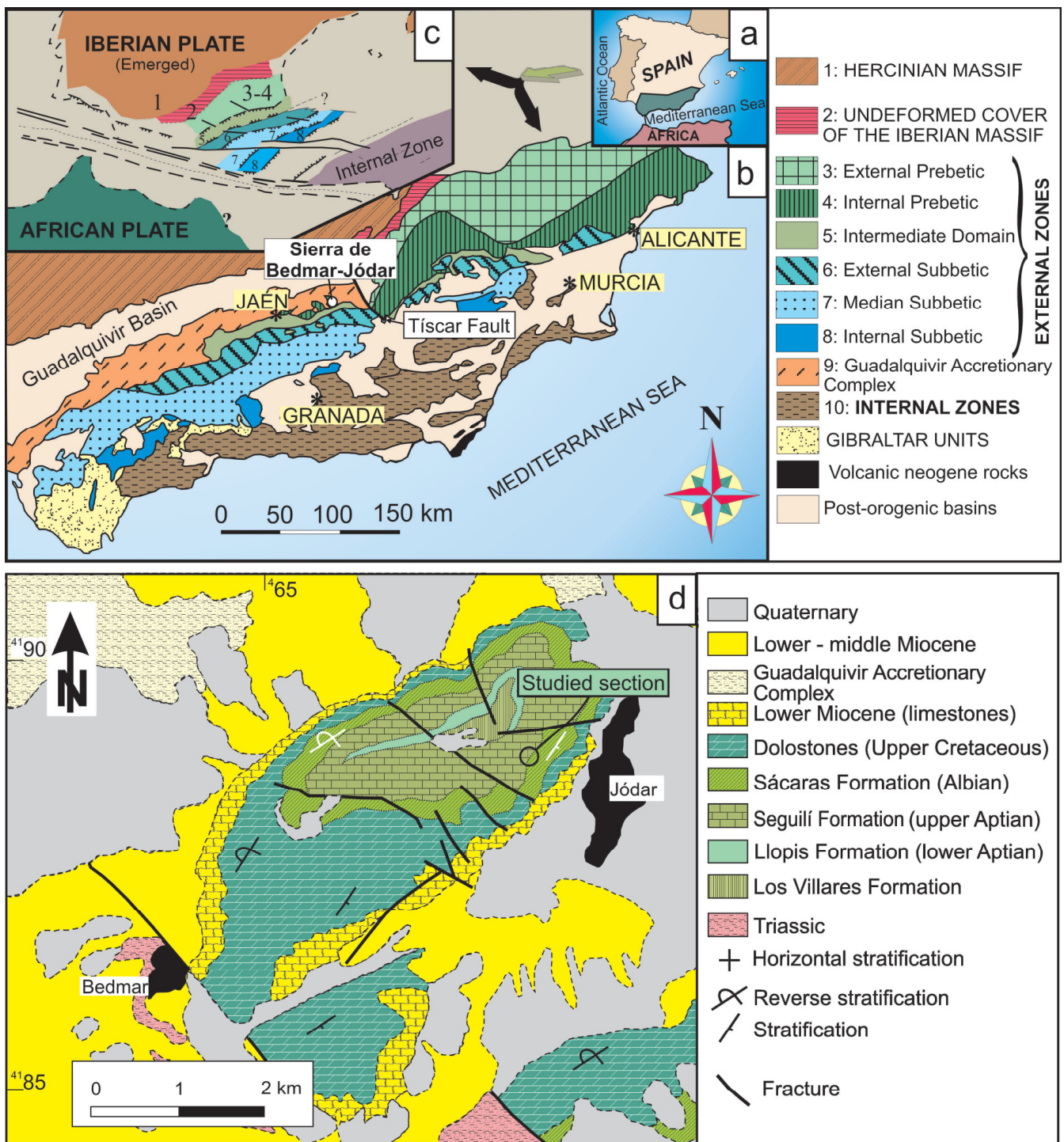


Figure 1. Geological setting of the Sierra de Bedmar-Jódar. (a) Location of the Betic Cordillera in the South of Spain. (b) Geological sketch of the Betics with position of the Sierra de Bedmar-Jódar, to the West of the Tíscar Fault. (c) Paleogeographic reconstruction of the South Iberian Margin for the Early Cretaceous. (d) Geological maps of the Sierra de Bedmar-Jódar with the location of the studied section.

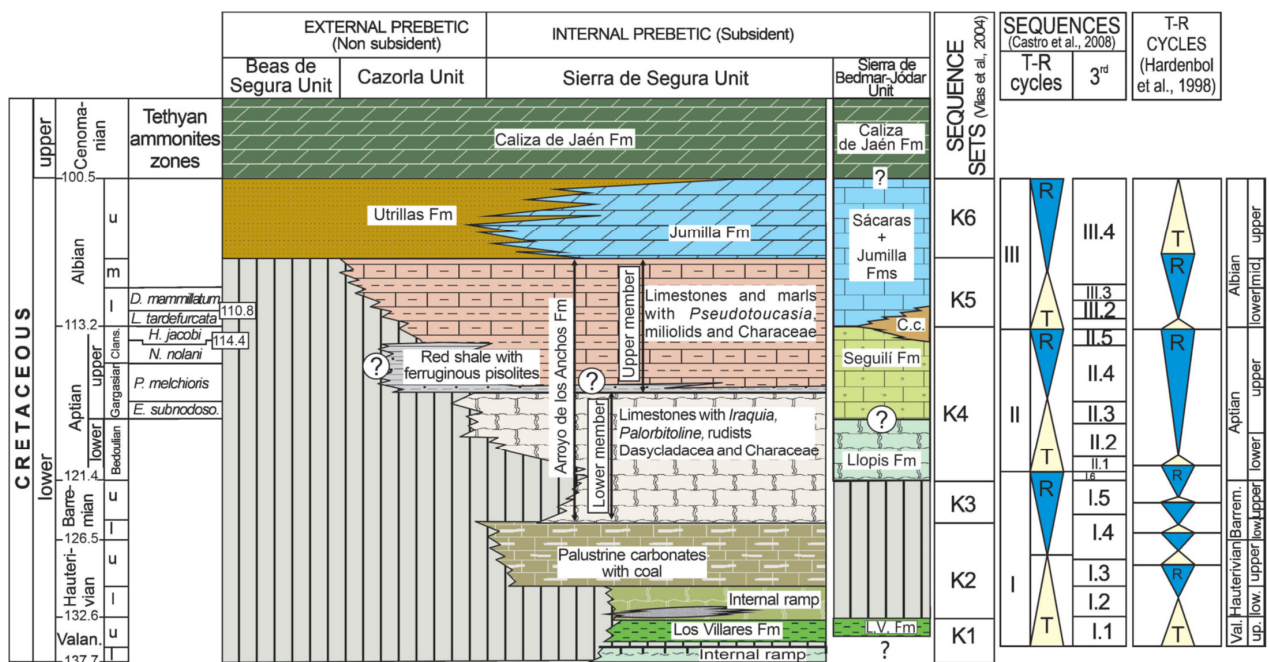


Figure 2. Chronostratigraphic chart of the Prebetic in the Cazorla-Segura outcrops and correlation with the Sierra de Bedmar-Jódar. The numerical ages (in Ma) and the Tethyan Ammonite Zones are from [25]. The sequence sets are from [14]. The chronostratigraphic record of these units is correlated with the sequences (T-R cycles and sequences of 3rd order) from [5] and the cycles of [26]. T-R: transgressive-regressive. C.c.: Continental carbonates. Fm: Formation. Fms: Formations. L.V. Fm: Los Villares Formation. Val.: Valanginian. up.: upper. low.: lower. mid.: middle.

3. Materials and Methods

A detailed logging bed-by-bed of the Bedmar-Jódar Aptian–Albian transition (Figure 3) has been performed including sampling of hard rock for thin sections and samples of marls for sieving. Twenty-five thin sections have been studied, with focus on the analysis of microfacies as well as microfossil assemblages using a Leica M205C stereoscopic microscope. The finest fraction was studied under the same stereoscopic microscope.

Bulk C- and O-isotope analyses of the carbonate fraction ($^{13}\text{C}_{\text{carb}}$) of the 27 collected samples were carried out at the Stable Isotope Laboratory of the Instituto de Geociencias, Universidad Complutense de Madrid, using a ThermoScientific MAT253 Isotope Ratio Mass Spectrometer (Waltham, MA, USA). Connected to a Kiel IV Carbonate Device. The international carbonate standard NBS-19, NBS-18 (National Bureau of Standards) and in-house standards were used to calibrate to Vienna PeeDee Belemnite (VPDB) [27]. All the isotope data are reported with the δ (‰) notation referred to the Vienna-Pee Dee Belemnite (VPDB) standard. Analytical error (1σ) averaged $\pm 0.01\%$ for both carbon and oxygen.

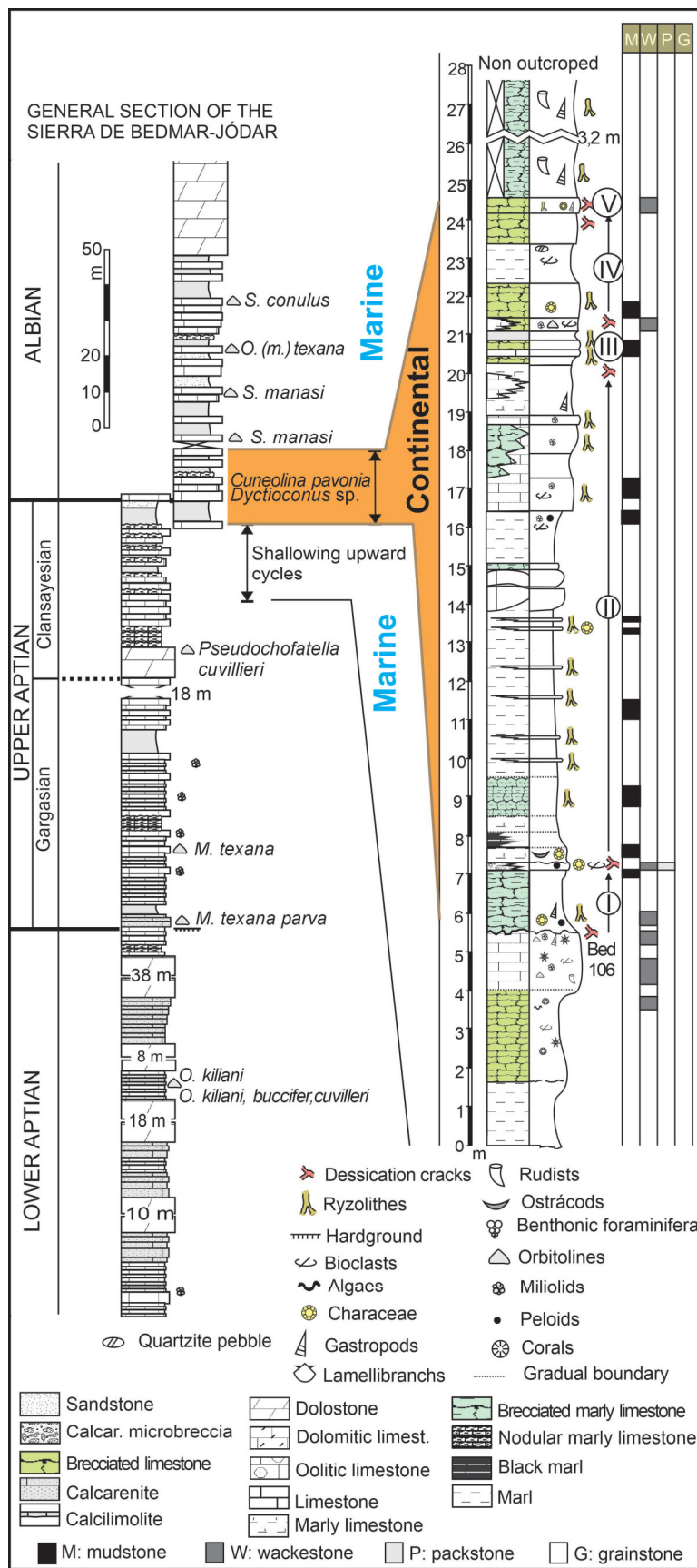


Figure 3. General stratigraphic section of the Aptian–Albian in the Sierra de Bedmar-Jódar and location of the detailed stratigraphic section of the continental carbonates.

4. Results

4.1. Facies and Microfacies

The carbonate sequences considered in this research crop out at the top of a shallowing-upward cycle that records the sedimentary evolution of a low-energy backreef lagoon developed in the latest Aptian (Seguilí Formation, [20]) (Figure 3). The topmost limestone bed of the Seguilí Formation (bed 106, Figures 3 and 4a–c) making the base of the studied succession, shows a microfacies of wackestone with miliolids, orbitolinids, and some poorly preserved gastropods and rudists. Besides, there are also some thin grains of quartz (<0.5 mm) and peloids. The fenestral texture is well developed. The top of this level, and therefore of the Seguilí Formation, shows desiccation cracks, borings (Figure 4d), and thin crusts of Fe-oxides. The geometry of this level shows a staggered shape controlled by small normal paleofaults of centimetric to metric slip (Figure 4a).

Over the bed 106, a carbonate succession 22.5-m thick crops-out (Figures 3 and 4a–c), made up by limestones and marly limestones with abundant rhizoliths (Figure 4e); in the upper part of the succession, there are several levels with rudists (Figure 4f). Six types of lithofacies have been recognized in this stratigraphic section:

1. Brecciated marly limestones with abundant rhizoliths filled with a yellow–brown sediment with a mudstone texture, stained by Fe oxides and frequently dolomitized. They have sub-circular cross-section with a cylindrical shape at a right angle related to stratification. The length of these rhizoliths is close to several centimeters and their diameter is no more than 1 cm. Some of these show downward bifurcations with decreasing diameters of second order branches.
2. Marly limestones with desiccation cracks, abundant in the bed tops. In the upper part of the section, these lithofacies show rounded quartzite clasts and black pebbles. Laterally, these materials can change to black marls facies, locally enriched in organic matter.
3. Limestones that laterally change to brecciated limestones or brecciated marly limestones. At the top of these lithofacies there are desiccation cracks. The rhizoliths are abundant and show similar features to the described in the lithofacies 1. Another feature of this lithofacies is that it is commonly more indurated than any other, and it is therefore very prominent at outcrop scale.
4. Limestones with orbitolinids that crop-out 7 m below the top of the studied section, in a bed 35 cm thick.
5. Marls with thin calcarenite levels no more than 10 cm thick, with lenticular morphology. There are abundant rhizoliths in the calcarenite beds; they have features similar to that described previously in the lithofacies 1.
6. Brecciated marly limestones with gastropods. In the upper part of the section there are rudists (*Mathesia darderi* (Astre)) (Figures 3 and 4f). The rhizoliths are abundant with similar features to the described in preceding facies.

Within these lithofacies there have been recognized seven types of microfacies (Table 1). The microfacies 1, azoic mudstone (Table 1; Figure 5a) is recorded in relation to the lithofacies 1 (brecciated marly-limestones) and lithofacies 3. The microfacies 2 and 3, mudstone and wackestone with Clavatoracea (charophytes), *Atopochara trivolvis* var. *trivolvis* Peck, *Clavator grovesii* var. *lusitanicus* Grambast-Fessard and tallus of charophyta *Munieria grambastii* Bystricky (Table 1, Figures 5b–d and 6) have been observed in the samples of the lithofacies 1, 3, 5, and 6. In this last lithofacies.

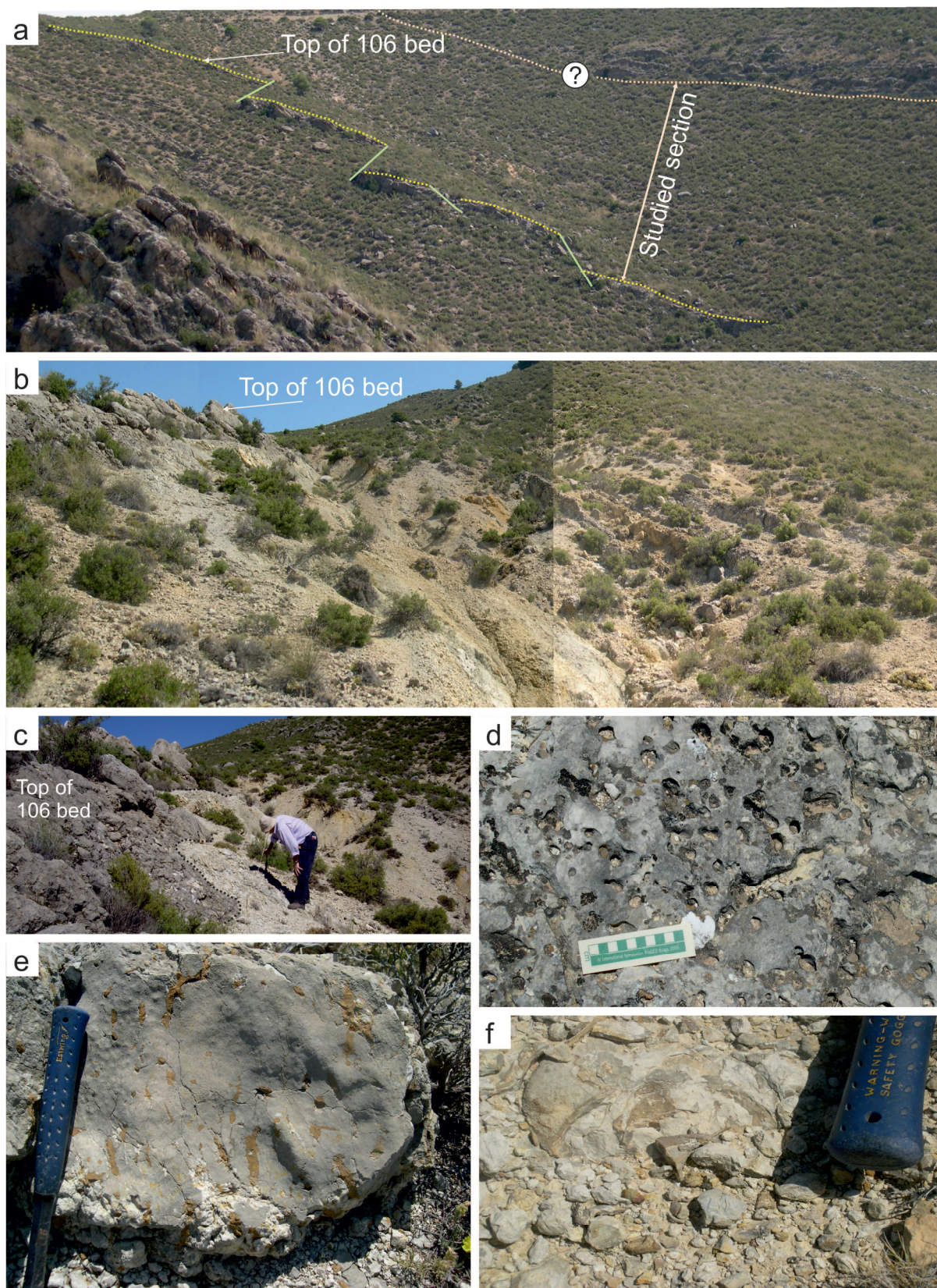


Figure 4. Features of the outcrops. (a,b) Panoramic view of the outcrop. The top of the 106 bed is remarked with the position of some paleofaults in (a,c). Irregular morphology of the top of the 106 bed. (d). Borings in the top of 106 bed. (e) Rizholiths (in brown color) in a limestone bed. (f) Rudists in nodular limestones.

Table 1. Microfacies observed in the studied stratigraphic section.

Microfacies N°	Grains	Fossils	Other Features	Environment	
1	Azoic Mudstone	Without grains	Without fossils	Desiccation cracks, bird-eyes, mottled texture	Restricted marine platform with subaerial episodes
2	Mudstone with characea	Peloids	Characeae, gastropod, bioclast	Desiccation cracks, mottled texture, ryzoliths.	Humid platform interior with subaerial episodes with desiccation cracks, mottled texture and ryzoliths development
3	Mudstone with miliolids	Peloids	Miliolids, bivalve bioclasts, Nodosaridae, ostracods	Few developed mottled texture, stained by FeO. Locally dolomitized	Restricted marine platform with low energy. Subaerial episodes with mottled texture development
4	Mudstone with ostracods	Without grains	Ostracods, characeae	Mottled texture	
5	Wackestone with characeae	Peloids	Miliolids, Orbitolinids	Thin quartz grains, mottled texture with curved cracks. Stained by FeO	Humid platform interior with subaerial episodes with desiccation cracks and mottled texture development
6	Wackestone with orbitolinids	Some peloids	Orbitolinids, miliolids, rudist bioclasts	Mottled texture stained by FeO. Curved cracks. Locally dolomitized	Open inner platform with subaerial episodes
7	Packstone with characea	Peloids	Characeae, bioclasts	Desiccation cracks, mottled texture. Locally brecciated texture	Humid platform interior with subaerial episodes with desiccation cracks and mottled texture development

Salpingoporella sp., has been detected (Figure 6). The packstone with charophytes (microfacies 4, Table 1; Figure 5e) is associated to the lithofacies 3 and 5, limestones that laterally change to brecciated limestones and marls with thin calcarenite levels, respectively. Microfacies 5, mudstone with miliolids (Table 1, Figure 5f) can be detected in the lithofacies 3. Mudstone with ostracods (microfacies 6, Table 1, Figure 5g) is related to marly limestones with desiccation cracks (lithofacies 2). Finally, the microfacies 7, wackestone with orbitolinids (*Mesorbitolina subconca* Leymerie) (Table 1 and Figures 3, 5h and 6) has been observed in lithofacies 4.

4.2. Sedimentary Sequences

Above the irregular surface, controlled by paleofaults, with desiccation cracks developed in subaerial conditions, at the top of bed 106 (Figures 3, 4a–c and 7), five shallowing upward elementary sequences (I to V in Figure 7) can be recognized, whose tops are also characterized by desiccation cracks. The thickness of each sequence ranges between 0.5 m (sequence V) and 13.25 m (sequence II).

Sequence I is 2-m thick (Figure 7). The lithofacies are brecciated marly limestones, with microfacies 3 (Table 1, Figure 5f) that laterally change to marly limestone and, at the top, to a level of limestone with microfacies 2, 3, or 4 (Table 1, Figure 5b,f,h). The top of this level shows desiccation cracks. Rhizoliths are present in both lithofacies with similar features as those described in the preceding heading.

Sequence II is 13.25 m thick (Figure 7). Three main lithofacies, marls, marly limestones, and limestones make up the sequence. These lithofacies change laterally to brecciated marly limestones. In the lower part of the sequence, some levels of marly limestones change laterally to black marls whose thickness is no more than 50 cm. Thin calcarenite lenticular levels with microfacies 2 (mudstone with charophytes, Table 1) appear intercalated in the marls. Rhizoliths are abundant in the calcarenites (Figure 7). The limestone facies, mudstone of miliolids with rhizoliths (microfacies 5, Table 1), occurs in the upper part of the sequence and is interfingering with marly limestones with gastropods. The top of the sequence shows desiccation cracks. On the basis of the calcarenite levels with rhizoliths (microfacies 2, Table 1, Figure 5b), ten small cycles are differentiated.

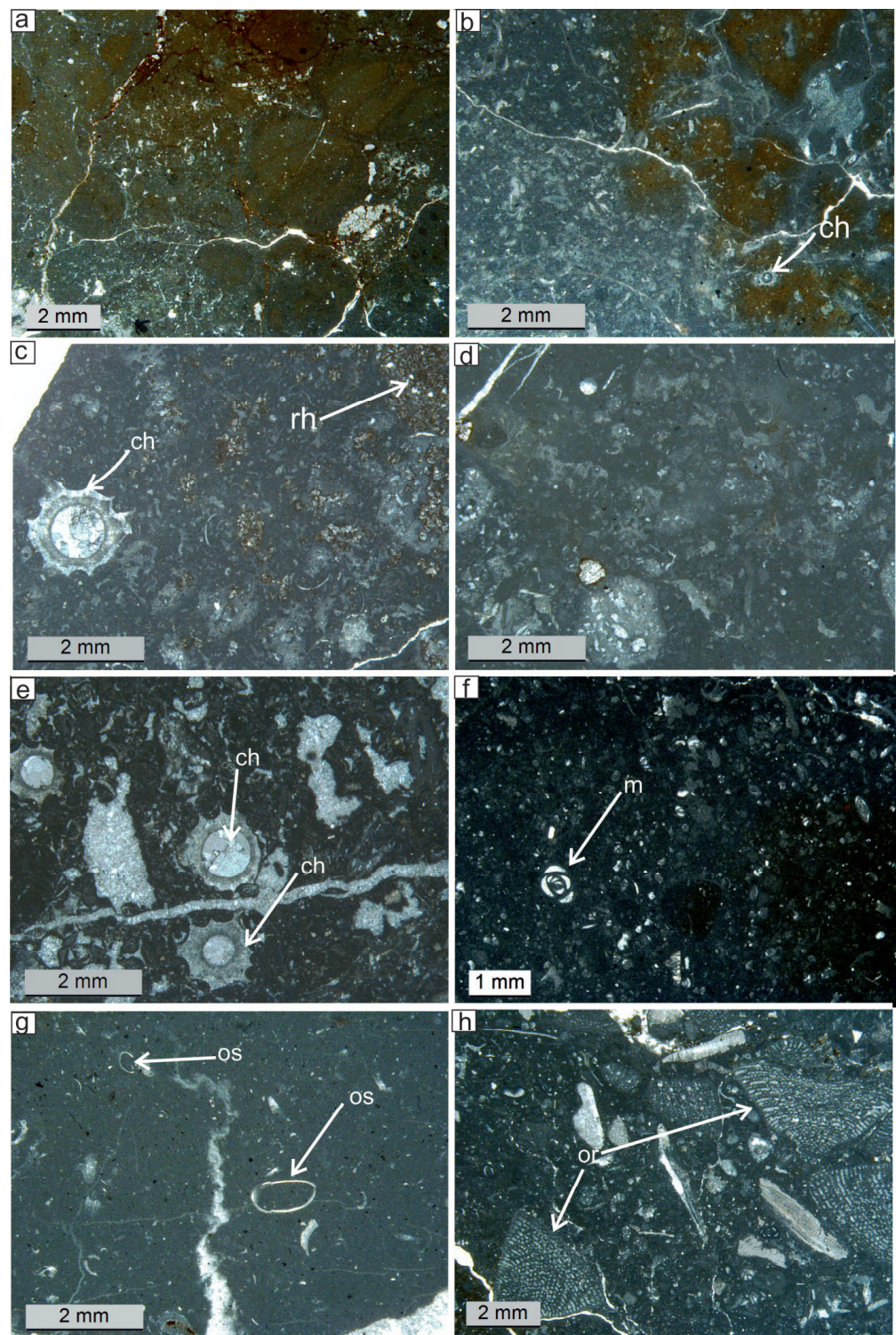


Figure 5. Microfacies recognized (according to the Table 1). (a) Microfacies 1: Azoic mudstone with desiccation cracks and mottled texture (RO-C-495). (b) Microfacies 2: Mudstone with charophytes (RO-C-485). (c) Microfacies 2: Mudstone with charophytes (RO-C-490) and rhizoliths. (d) Microfacies 3: Wackestone with charophytes (RO-C-476). (e) Microfacies 4: Packstone with charophytes (RO-C-480). (f) Microfacies 5: Mudstone with miliolids (RO-C-492). (g) Microfacies 6: Mudstone with ostracods (RO-C-482). (h) Microfacies 7: Wackestone with orbitolinids (RO-C-498). For all the images: ch: charophyte; rh: rhizolith; m: miliolid; os: ostracod; or: orbitolinid.

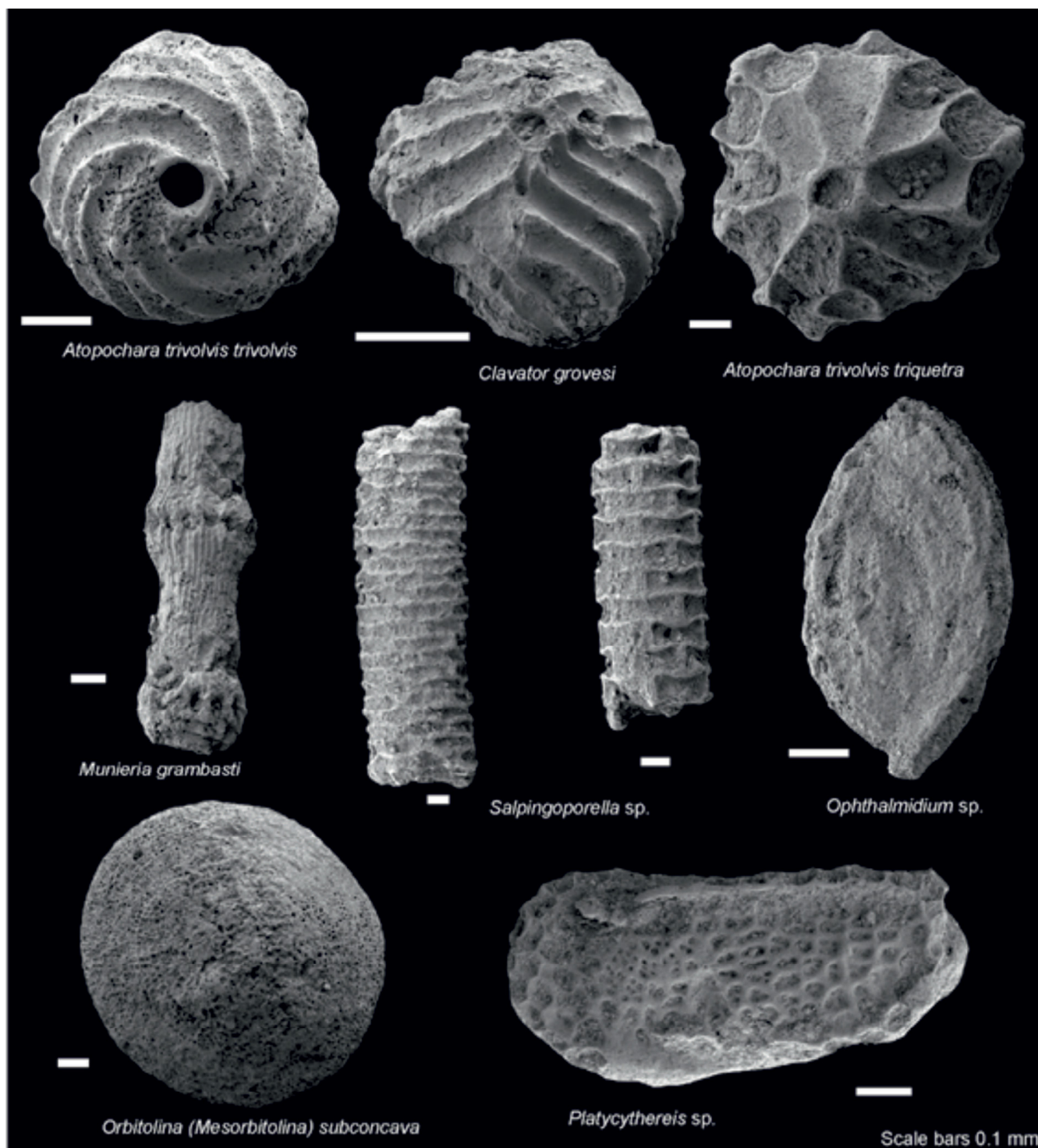


Figure 6. Microfossils in the analyzed stratigraphic section.

Sequence III has a thickness of 1.5 m (Figure 7). Limestones, brecciated limestones, marls, and marly limestones that laterally change to brecciated limestones make up this sequence. The rhizoliths are abundant in all the lithofacies. Four small cycles (Figure 7) with a shallowing upward trend capped by rhizoliths in the top, can be differentiated. The microfacies of the two lower small cycles is azoic mudstone (without grains and fossils, microfacies 1, Table 1; Figure 5a). The uppermost small cycle has microfacies 7 (wackestone with orbitolinids; Table 1, Figure 5h), and abundant rhizoliths and desiccation cracks in their top.

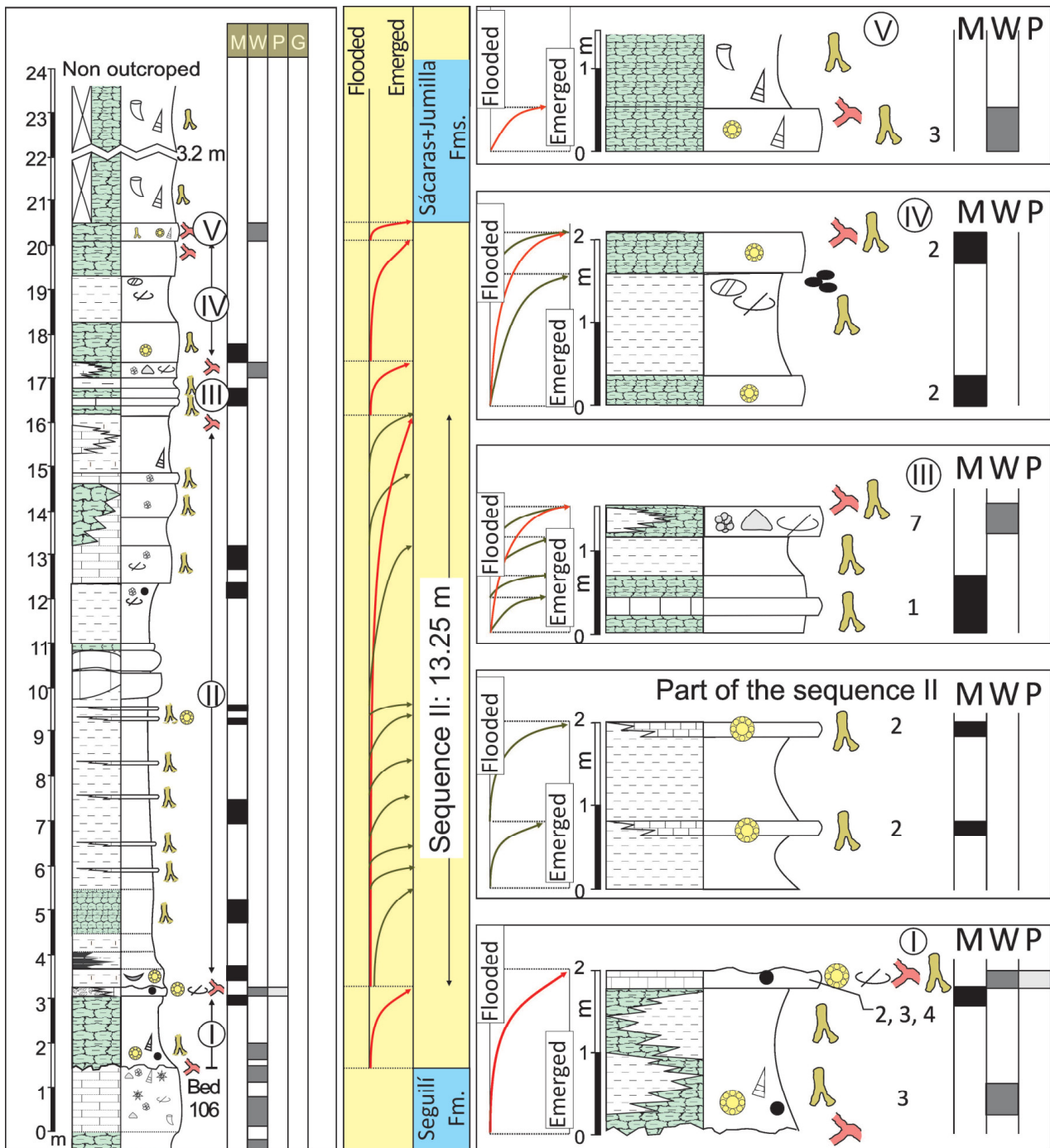


Figure 7. Sequences considered in the studied section. To see the Figure 3 for the symbols of components of the rocks. The numbers correspond to the microfacies in the Table 1.

Brecciated limestones and marly limestones are the lithofacies making up the 2.10 m thick sequence IV (Figure 7). The microfacies of the brecciated limestones is mudstone with charophytes. The top of the marly limestone shows rhizoliths, quartzite pebbles, and black pebbles, which allow to distinguish two small cycles in this sequence (Figure 7) bounded by the top of the marly limestones. Brecciated limestones with microfacies 2 (Table 1) make up the uppermost small cycle. At their top, rhizoliths and desiccation cracks occur. Sequence V is 0.5 m thick (Figure 7). It is made up of brecciated limestones with microfacies of wackestone with charophytes. As in other sequences, rhizoliths and desiccation cracks

are abundant at the top of the sequence. Over this last sequence brecciated marly limestones with rudists and gastropods, and also with abundant rhizoliths, crop out.

4.3. Biostratigraphy

The presence of *Mesorbitolina subconca* in bed 106 (lower part of the studied section) and in the top of the elementary sequence III, *Pseudochofatella cuvillieri* Deloffre in the upper part of the Seguilí Formation, and *Simplorbitolina manasi* Ciry and Rat in the base of the Sácaras Formation (Figure 3) indicates that these sediments were deposited in the Aptian–Albian transition [28]. These authors consider that the presence of these orbitolinids define the biostratigraphic units 4 and 5, correlated with the *Hypacanthoplites jacobi* Collet (*H. jacobi*) and *Leymeriella tardefurcata* Laymerie (*L. tardefurcata*) ammonite zones, that comprise the Aptian–Albian transition. Additionally, the charophyte association (*Atopochara trivolvis* var. *trivolvis*, *Clavator grovesii* var. *lusitanicus* and *Munieria grambastii*; Figure 6) present in these sediments is also characteristic of this time interval [29,30].

4.4. C and O Stable Isotopes

Table 2 shows the values of the isotopic C and O ratios coming from the analysis of the bulk samples taken for this study. Besides, Figure 8 depicts the profile of $\delta^{13}\text{C}$ and Figure 9 shows the correlation between the isotopic values $\delta^{13}\text{C}$ and $\delta^{18}\text{O}$. The value of the correlation coefficient R^2 is 0.179 (Figure 9). However, for $R = 0.424$ and $t = 2.343$ (Student's test), the correlation between $\delta^{13}\text{C}$ and $\delta^{18}\text{O}$ will be significant with a probability of 95% ($t = 2.05$ for 27 analyses) and insignificant with a probability of 99% ($t = 2.77$ for 27 analyses), only there is an anomalous sample (RO-C-484). Without this sample, the correlation is insignificant ($R = 0.062$, $t = 0.305$ for 26 samples).

Table 2. Values of the $\delta^{13}\text{C}$ and $\delta^{18}\text{O}$ in each sample taken in the studied stratigraphic section.

Samples	$\delta^{13}\text{C}$	$\delta^{18}\text{O}$
RO-C-476	0.34	−2.81
RO-C-477	−1.38	−2.42
RO-C-478	−1.94	−2.59
RO-C-479	−3.16	−2.47
RO-C-479B	−2.53	−2.86
RO-C-480	−2.72	−1.97
RO-C-481	−2.58	−2.10
RO-C-481b	−2.89	−2.26
RO-C-482	−1.72	−1.64
RO-C-483	−4.57	−2.16
RO-C-484	−6.81	−3.85
RO-C-485	−0.51	−1.29
RO-C-486	−3.40	−2.44
RO-C-487	−0.83	−2.19
RO-C-488	−1.82	−2.56
RO-C-489	0.16	−1.84
RO-C-490	0.44	−2.35
RO-C-491	−0.05	−2.16
RO-C-492	−0.33	−2.43
RO-C-493	−1.35	−2.34
RO-C-494	−1.55	−2.85
RO-C-495	−1.19	−2.52
RO-C-496	0.87	−2.53
RO-C-497	−2.09	−2.95
RO-C-498	−1.09	−2.36
RO-C-499	−1.09	−2.09
RO-C-500	−1.34	−2.50

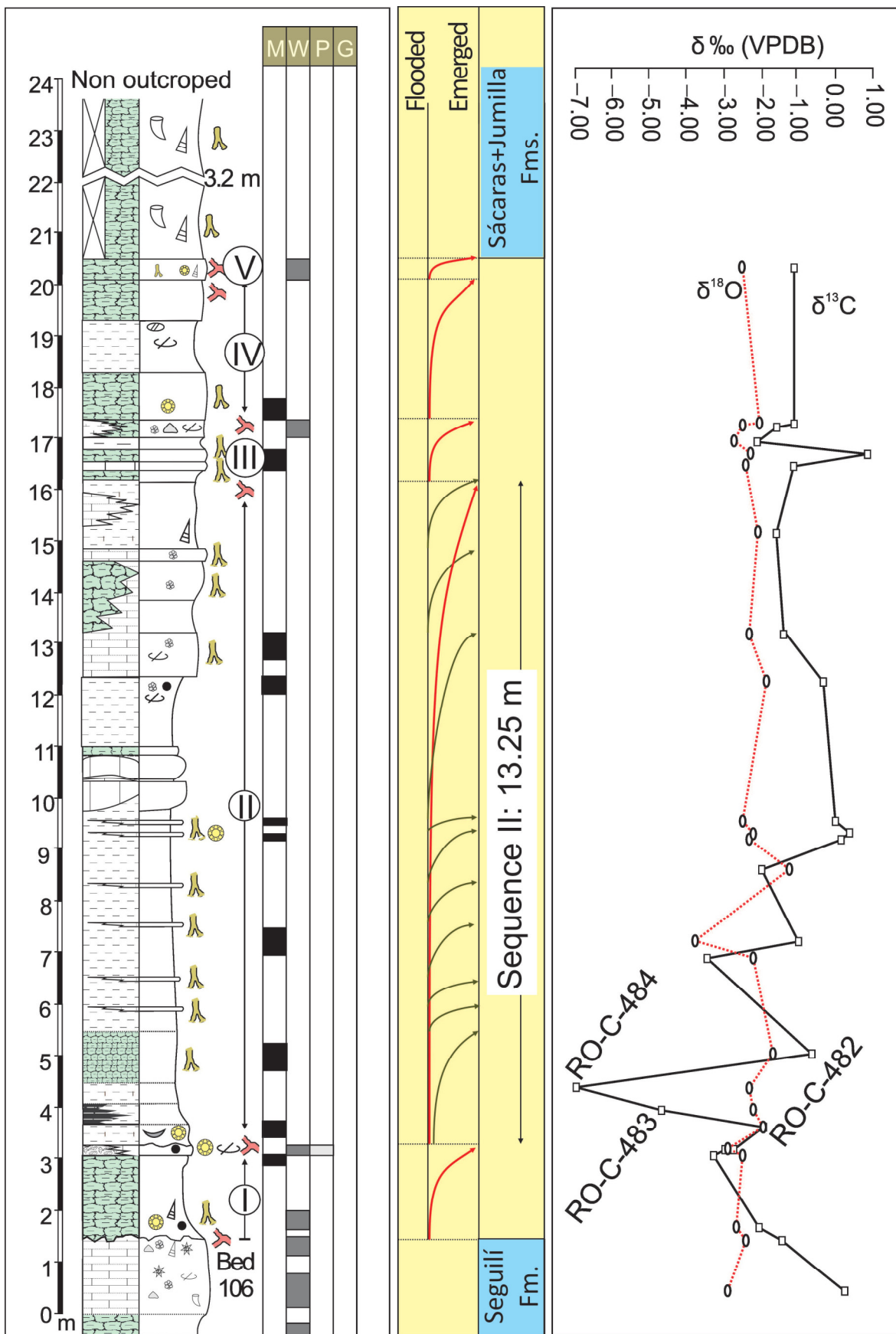


Figure 8. Stratigraphic section with sequences and isotope data ($\delta^{13}\text{C}$ and $\delta^{18}\text{O}$, both ‰ VPDB; see text for more details).

While the $\delta^{18}\text{O}$ values are around the published Aptian and Albian marine values ($\delta^{18}\text{O} = -2\text{‰}$; [31]), the $\delta^{13}\text{C}$ shows negative values, far from the marine value for this ratio proposed by the same author for that time interval ($\delta^{13}\text{C} = 2\text{‰}$, [31]). The lower and higher values of $\delta^{13}\text{C}$ are -6.81‰ and 0.87‰ respectively (standard deviation 1.65‰), with an average value of -1.67‰ . The $\delta^{18}\text{O}$ values range between -3.85‰ and -1.29‰ (Table 2) and their average value is -2.39‰ (standard deviation 0.47‰). The strong negative $\delta^{13}\text{C}$ shifts detected from the sample RO-C-483 and 484 (both samples are black marls), whose values are -4.57 and -6.81 respectively (Table 2 and Figure 8) must be emphasized.

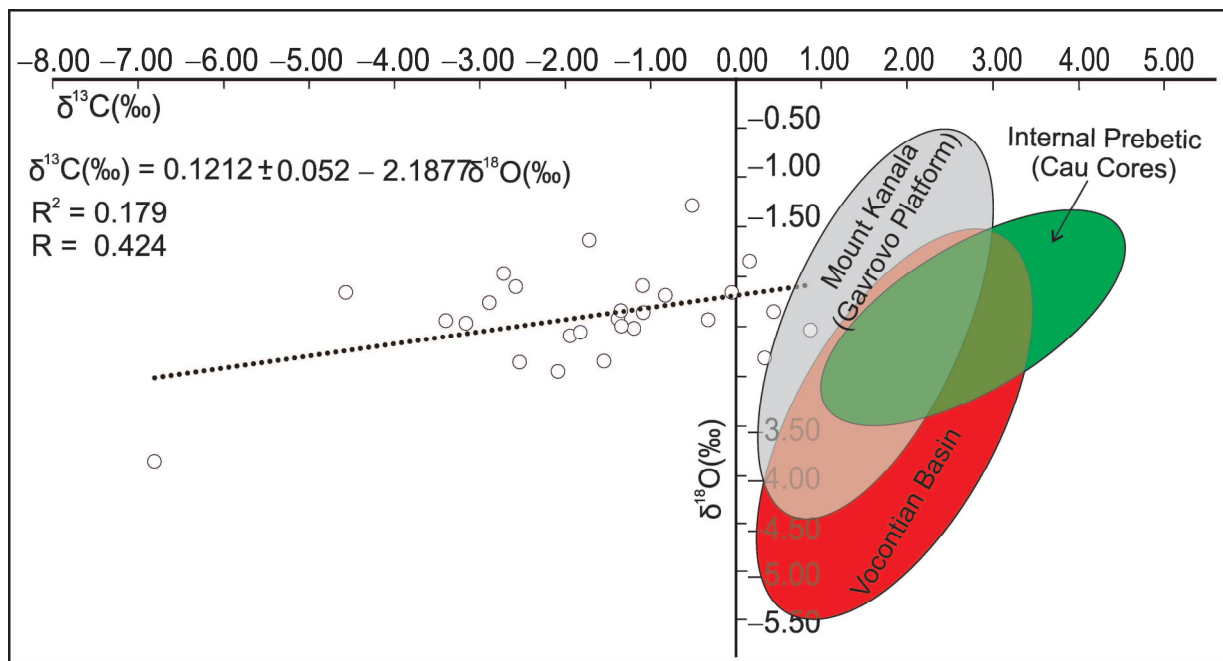


Figure 9. Correlation between the values of $\delta^{13}\text{C}$ (‰ VPDB) and $\delta^{18}\text{O}$ (‰ VPDB) with indication of correlation straight (see text for more details). In red color, the field of isotope ratios from the Vocontian Basin [32], in grey color from the Mount Kanala in the Gavrovo platform [33] and in green color from the Internal Prebetic (Cau Cores, outer platform, Aptian) [34].

5. Discussion

5.1. Sedimentary Environment

At a global scale, the Aptian–Albian transition has been characterized by important paleogeographic changes related to the Central Atlantic rifting stage [7] and with climatic changes marked by short duration episodes where warm and cold climates alternate [2,11,35–37]. In the SICM, a shallow platform on a fault block tilted to the NE was developed which at present crops out in the Sierra de Bedmar-Jódar, which is similar to that described by other authors on the southern margin of the Alpine Tethys with a clear evidence of extensional tectonics [7,37–40]. The Sierra de Bedmar-Jódar belongs to the so-called Prebetic of Jaén, made by isolated outcrops without apparent connection to the rest of the Prebetic platform [6,19–24]. Tectonics was an important factor controlling the sedimentation, as can be evidenced by the small faults affecting the bed number 106 (Figure 4a) of the studied succession. A small-scale graben was developed and, simultaneously, a relative sea level fall occurred. Consequently, continental environments were established on the emerged areas with development of palustrine facies. However, these continental environments were probably sensitive to relative sea level changes and to the fluctuations on the piezometric level. Locally, some ponds were developed, where organic matter accumulation occurred with the formation of black marls and marly limestones (Figure 10).

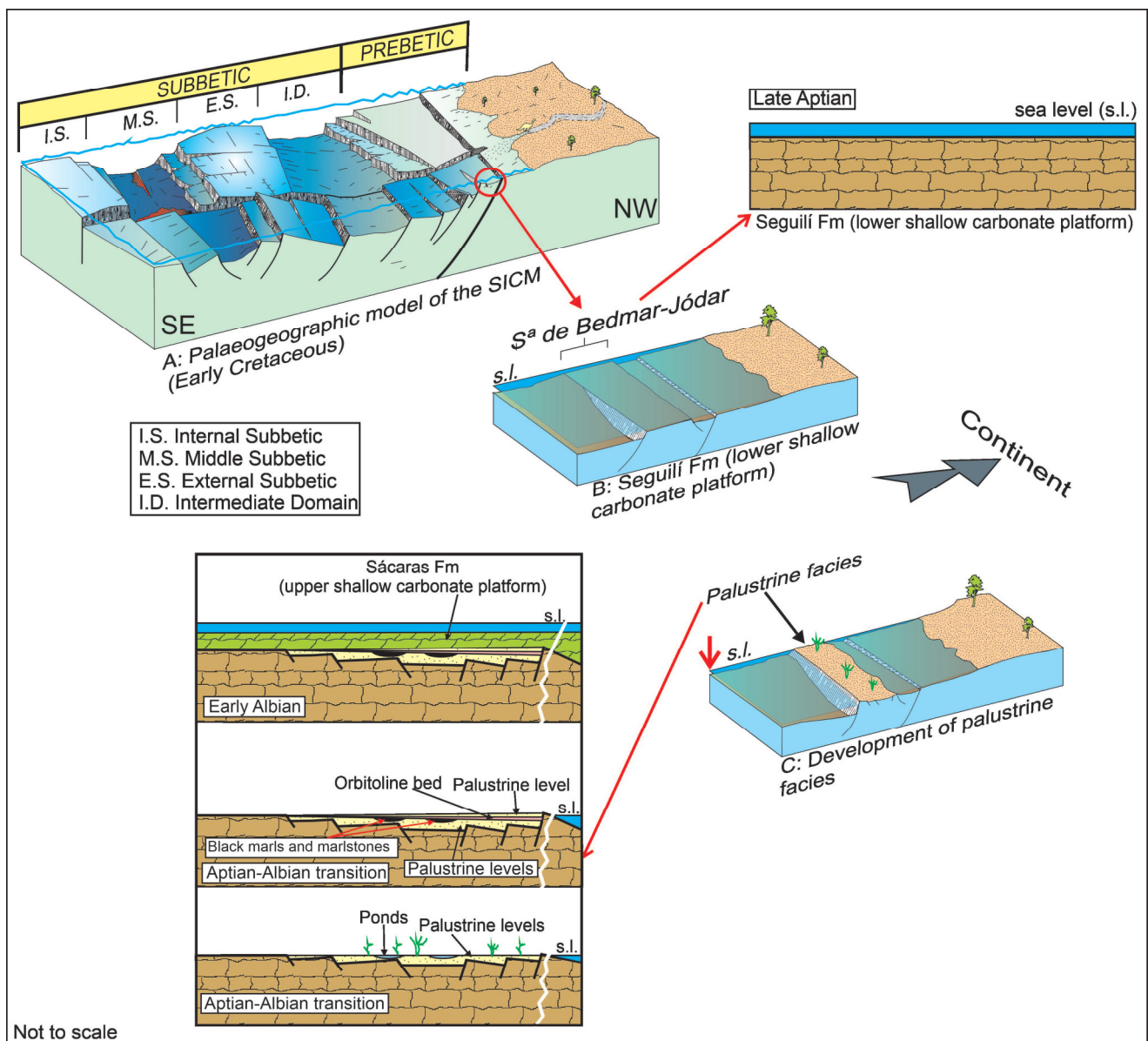


Figure 10. After that, a new relative sea level fall drove to the development of new palustrine facies with rhizoliths and charophytes. The presence of quartzite-rounded clasts in these materials is probably an evidence pointing to tectonic episodes as the cause of these relative sea-level changes making erosion in the continental hinterland [5,41].

It is important to note that in the upper part of the continental succession there are brecciated marly limestones with rhizoliths and clavatoracea charophytes (*Atopochara trivolvis* var. *trivolvis*; Figure 6), but also with marine fossils as dasycladaceae (*Salpingoporella* sp.; Figure 6), orbitolinids, marine gastropods, and rudists. This was the result of the change from marine sediments developed in the inner part of a carbonate platform that was exposed to subaerial conditions. Besides, a vegetal cover was developed. Their roots made up the rhizoliths and, locally, charophytes grew in the fresh-water ponds (Figure 10).

The presence of *Atopochara trivolvis* var. *trivolvis* and *Clavator grovesii* var. *lusitanicus* indicates that the waters could have a wide range of salinity, from fresh to brine waters, which is corroborated by the presence of miliolids and *Salpingoporella* sp. These charophytes are common in coastal ponds enriched in organic matter from the Escucha Formation (Iberian Chain) and in the Montsec (Central Pyrenees) [29,30]. These environments occurred

during a relative sea-level lowstand stage, with development of pedogenic processes that affected the emerged coastal marine sediments [42].

5.2. Sedimentary Sequences

The sedimentary sequences shown in this research can be considered as medium-scale sequences [43]. In addition, within some of these, there can be differentiated smaller-scale cycles of metric thickness (Figure 7) that can be considered as elementary sequences [43]. This nomenclature is descriptive; it does not imply any time range, as the time framework is not well-known for each sequence.

As it was established previously, each shallowing upward elementary sequence is made up by smaller cycles of metric thickness. There are 18 smaller cycles in total. Correlation with ammonite zones indicates that the studied interval represents the *H. jacobi* (latest Aptian—earliest Albian) to *L. tardefurcata* (late early Albian) zones, as it is shown in the biostratigraphic heading. The age of the bottom of the *H. jacobi* Zone is 114.40 Ma and the top of *L. tardefurcata* is dated as 110.8 Ma [25], so the time represented by the five shallowing upward elementary sequences would be at least 3.60 Ma. Following this reference, each one of the 18 smaller cycles would be equivalent to 0.20 Ma in average. From these data and considering the thickness of the studied section (22.5 m), the resulted average sedimentation rate is 0.625 cm/ka. This sedimentation rate is very low compared with that proposed for carbonate palustrine/lacustrine environments, with values between 9 cm/ka and 3 cm/ka [44].

These low sedimentation rates can result from the successive emersion episodes that affected the area, up to five times along the 3.6 Ma interval, coinciding with the top of the described elementary sequences. Each emersion episode resulted in the development of subaerial surfaces with desiccation cracks, plants growth, pedogenic conditions, and locally ephemeral ponds. Besides, carbonate production stopped at least five times, coinciding with discontinuities associated to the top of each one of the described elemental sequences. Each interruption was associated to emersion and the implantation of continental environments, that is, there were sudden drops in relative sea level, leaving the lagoon bottom emerged, on which subaerial plants grew, with the development of pedogenic conditions.

5.3. Isotopic Data Interpretation

In the Vocontian Basin (France), several authors [4,32,45,46] show values of $\delta^{13}\text{C}$ between 0.65‰ and 2.32‰, while $\delta^{18}\text{O}$ change between -5‰ and -1.9‰ , in rocks occurring between the lower part of the Kilian level and the top of the Paquier level, with an Aptian—Albian transition age. The interval between the upper part of the *R. angustus* (NC7) and the lower part of the *P. columnata* (NC8) nannofossil zones (correlated with the upper and lower parts respectively of the ammonite zones *H. jacobi* and *L. tardefurcata*) shows values of $\delta^{13}\text{C}$ between 2.5‰ and 4‰ [10]. For the Barremian—Albian of Mt. Kanala section (Gavrovo platform, western Greece [33]), made up by shallow-water carbonates with clear evidence of diagenetic and pedogenetic processes, the $\delta^{13}\text{C}$ values lie in a range from -1‰ to 3.5‰, and $\delta^{18}\text{O}$ data from -4.78‰ to 0.38‰. For the Aptian—Albian transition, it has been shown that $\delta^{13}\text{C}$ values oscillate between 1‰ and 3‰ [33]. The rocks of the Ionian Basin [47], dated as Aptian—Albian transition, although with low biostratigraphic accuracy, show $\delta^{13}\text{C}$ values in a range from 2.6‰ to 3.9‰, and values of the $\delta^{18}\text{O}$ that range between -1.5‰ and -0.3‰ . The hemipelagic sediments of the Almadich Formation recorded in the Cau Core show values for the upper Aptian of $\delta^{13}\text{C}$ between 1.25‰ and 4.5‰ and between -3.25‰ and -1.25‰ for $\delta^{18}\text{O}$; however, there are no data for the Aptian—Albian transition from these rocks [34].

The highest and lowest values of the $\delta^{13}\text{C}$, 0.87, and -6.81‰ respectively from the samples of this study, are lower than data from Vocontian Basin, Gavrovo platform, or Ionian Basin [10,32,33,47] (Figure 9). The samples with the most negative $\delta^{13}\text{C}$ signature are recorded in the black marl levels. Probably, they represent a more intense diagenetic overprint that samples with less negative values [33], but the original C-isotope ratio probably

reflected negative values related to the presence of organic matter in these rocks [32,34,47]. Early diagenesis and edaphic processes could be responsible for the broader spread of these data. With respect to the extreme values of $\delta^{18}\text{O}$, -1.29‰ and -3.85‰ , they are in the range shown by rocks from the basins quoted previously [32–34] and also close to the data from the Ionian Basin [47] for this isotope relation.

5.4. Correlation with Other Prebetic Areas

The materials studied in this research are stratigraphically located between the Seguí and Sácaras + Jumilla Formations (Figure 2), in the Aptian–Albian transition. In the Prebetic Zone, the Aptian–Albian transition coincides with the limit between the K4 and K5 sedimentary episodes [6,14]. The K4 episode was characterized by the development of the Urganian platforms; its upper limit is a discontinuity in which part of the latest Aptian and earliest Albian are not recorded. The K5 episode is characterized by important changes in thickness and facies, especially those interpreted as deposited in mixed platforms. In the Sierra de Segura Unit (Figure 2), the boundary between episodes K4 and K5 is located within the upper member of the Arroyo de los Anchos Formation [20,48,49]. This lithostratigraphic unit is characterized by the development of carbonates deposited in the inner platform, with the development of marsh and supra-tidal facies and some terrigenous beds intercalated. These deposits took place during the last episode of the Atlantic rifting [20,48,49]. In slightly subsiding contexts or in raised blocks, the record is made up by a succession of clays with ferruginous pisolites, followed by green marls [41]. In more subsiding sectors, it is represented by carbonaceous limestones with pseudotoucasia overlaid by sands and carbonates with ostreids. In short, in the Sierra de Segura Unit, in the Aptian–Albian transition, marsh facies with earliest subaerial weathering processes (ferruginous pisolites) are intercalated with shallow marine carbonate levels, which could be related with high frequency fluctuations in relative sea level. The better preservation of the pedogenic levels in the Sierra de Bedmar-Jódar, in which there is a clear development of marsh facies, punctually interrupted by thin levels of orbitolinid limestones, could be explained in relation to local factors. Among them, the most important was the development of a tectonic graben generated by small faults, presently clearly visible affecting level 106, which forms the base of the studied sequence. The development of this structure, favored subsidence and accumulation of this type of deposits at the same time that it contributed to their preservation in the succeeding rises of the relative sea level. From a regional perspective, this could be interpreted as the result of a significant drop in sea level, related to tectonic processes with the development of the isolated block during the Aptian–Albian, and which could be also associated with the Atlantic rifting episode [7,37–40].

In the Prebetic of Alicante, the Aptian–Albian transition coincides with the limit between the transgressive-regressive (T-R) II and III cycles [5] (Figure 2). More specifically, this limit coincides with that of the third order cycles II.5, regressive, and III.1, transgressive (Figure 2). Cycles II.5 and III.1 record a sudden increase in the subsidence rate, as it is shown by the greater thickness of these cycles with respect to II.4. In addition, the lateral changes in thickness were more marked during the sedimentation of II.5 and III.1, which was related to the record of a local extensional tectonic event [5]. This event led to the formation of local grabens, with marine sedimentation in distal parts of the platform (the Prebetic of Alicante), whereas in more proximal parts of the platform these subsiding areas were occupied by fresh water that favored the development of the marsh facies, in a general context of relative sea level drop. Outside these highly subsident grabens, the Aptian–Albian transition in the Prebetic platform is represented by a discontinuity, probably related to emersion. The third order cycle III records a further transgressive-regressive cycle, with littoral to continental deposits in the proximal sectors of the Prebetic that grade to the distal sectors, as Sierra de Bedmar-Jódar and the Prebetic of Alicante, to mixed terrigenous-carbonate platform environments (Sácaras Formation), followed by the development of a shallow carbonate platform with rudists during the upper Albian (Jumilla Formation).

5.5. *The Demise of the Carbonate Platform*

The latest Aptian-earliest Albian transition records the last episode of demise of carbonate platforms in the northern Tethys [11]. At a global scale, an Oceanic Anoxic Event occurred (OAE 1b, or Paquier level; [50]), with widespread deposition of organic-rich and biosiliceous sediments in open marine environments, interpreted as related to a phase of increased nutrient input and enhanced primary productivity [11,37,51–53]. Besides, this time interval has been associated with repetitive dys- to anaerobic conditions along the northern Tethyan margin, in the central Tethys and partly also in the Atlantic [1,2,11,54–57].

Some authors have shown that the Aptian–Albian transition was characterized by a complex climatic history and considerable palaeoceanographic perturbations [2,35,45,54,58]. Other authors [55] argued the development of a phase of global warming, frequently related to volcanic activity due to the South Kerguelen and Nauru-Mariana LIPs. Several hyperthermals have been recognized across the Aptian–Albian boundary interval, which were inserted in a general global warming context, which they also related to the development of the previous LIPs [56]. According to this last idea, the base of the Albian has been interpreted as a warm, humid period, with considerable freshwater flow into the ocean, decreasing its surface salinity [35,45,51,59] (see review in [11]). On the other hand, it has been also proposed a brief interval of global climate cooling sufficiently for winter snow and ice to return to the polar regions in the late Aptian and Early Albian [1,60].

For the Aptian–Albian boundary and admitting a phase of global warming, several researchers [55–57] estimated that a rise in sea level of medium amplitude took place. In spite of the general sea level rise quoted for the Mediterranean Tethys domain, the conditions that are deduced from the study of the sedimentary record of the Sierra de Bedmar-Jódar, configured in this time interval as an isolated carbonate platform in the SICM, show us that the development of palustrine and pedogenic conditions indicate a relative drop in sea level, which, ultimately, was responsible for the demise of the platform represented by the Seguilí Formation. This local drop in the sea level conditions could be the consequence of the rifting tectonic that affected the isolated block provoking the partial emersion. Other parts of the Prebetic platform were also affected by the tectonic [5], as well as the SICM [6,14]. In the Sierra de Segura Unit, the Aptian–Albian transition contains the record of marsh and supratidal carbonates, which are interpreted as related to an intense extensional tectonic phase, that gave rise to an important regression [48,49]. These features are interestingly similar to those that were highlighted from the Cretaceous shallow water succession outcropping in NW Sicily fold and thrust belt (i.e., the Panormide platform [37,40,53]). In these areas lacustrine clays were deposited, during the Aptian–Albian boundary, and mark the demise of the Lower Cretaceous carbonate platform and the rebirth of the Upper Cretaceous platform [37,53]. In the pelagic sedimentary record of the SICM, the Aptian–Albian transition is not represented because a regional event (E11) led to a stratigraphic unconformity with an associated hiatus embracing from the end of late Aptian to the early part of the middle Albian [16].

In this setting of intense tectonic activity, with regional sea level oscillations, pedogenic processes affected the sediments in palustrine environments and, probably, they were responsible for the diagenetic alteration of the C isotope ratio. This evolution can be explained as the result of very high frequency sea level regressions, which leave the shallow platform deposits regularly exposed to subaerial conditions with the development of vegetation typical of subaerial contexts, that settled over them (Figure 10). Besides, in somewhat more depressed areas, small swamps with poorly oxygenated waters were developed (Figure 10). The palustrine deposits of this isolated carbonate platform could be also associated with a significant change in regional hydrology driven by an increase in magnitude and frequency of rainfall events. These high-frequency sea level fluctuations are the consequence of continuous tectonic pulses that raised the isolated block that made up the Sierra de Bedmar-Jódar in that time interval and that, in short, were the cause of the demise of the platform represented by the Seguilí Formation. The ultimate preservation of the record of the palustrine and pedogenic deposits in the studied section, with respect

to other areas of the SICM, was favored by the depressed topography originated by the observed faults affecting the studied deposits, which configured a small paleo-trough.

6. Conclusions

A stratigraphic succession of shallow-water and continental carbonates of the Aptian–Albian transition, which belongs to the Prebetic of Jaén is analyzed. The Prebetic of Jaén has Cretaceous sedimentary sequences similar to other Internal Prebetic areas in an extensional geodynamic context of an isolated carbonate platform controlled by faults. However, in the Sierra de Bedmar-Jódar, the most important feature during the Aptian–Albian transition is the presence of a continental record of palustrine sediments with paleosols, covering sediments deposited in a carbonate platform. After the analysis of the stratigraphy, sedimentology and paleontology of this palustrine sediments and of their meaning in the evolution of this area of the SICM, we propose a demise model of carbonate platforms, which differs from that proposed for other Tethys perimediterranean platforms.

The cause of the demise of the platform was an extensive tectonic event, concomitant to a relative drop in the sea level of a regional amplitude, which in the studied area gave rise to a record of marsh sedimentation, with fresh water and successive entries of sea water. This record is exceptional in the SICM and in the Prebetic platform, where in general there is a discontinuity in the Aptian–Albian transition. The succession studied in this research allows to understand the environmental conditions in the Aptian–Albian transition, with a humid climate with significant fresh water inputs, which favored the development of aquatic organisms such as the charophytes. The subaerial exposure and diagenesis could have changed the original C isotope ratio of these sediments. The exceptional preservation of the studied lacustrine facies was related to the development of grabens or semi-grabens, in a general geodynamic context characterized by extensional faults that gave rise to tilted blocks.

Author Contributions: Conceptualization, J.M.M., L.M.N. and P.A.R.-O. Methodology; field section and sampling, J.M.M., L.M.N. and P.A.R.-O. Biostratigraphy: J.M.C., G.A.d.G. and M.R. Writing—original draft preparation, L.M.N., J.M.M. and P.A.R.-O. Writing—review and editing, all authors. All authors have read and agreed to the published version of the manuscript.

Funding: This research was funded by Project CGL2014-55274-P (Secretaría de Estado de I+D+i, Spain) and by the Research Group RNM-200 (Junta de Andalucía).

Acknowledgments: Our acknowledgement to Antonio Piedra-Martínez, Technician of the Laboratory of Geology (University of Jaén). The charophytes were classified with the help of C. Martín-Closas; we are very grateful by their suggestions. The comments of Dra Alonso-Zarza and collaborators in a visit to the crops-out analyzed in this research is also acknowledged. The proposals, corrections and comments of five anonymous reviewers have improved this manuscript.

Conflicts of Interest: The authors declare no conflict of interest.

References

1. Trabucho Alexandre, J.; van Gilst, R.I.; Rodríguez-López, J.P.; de Boer, P.L. The sedimentary expression of oceanic anoxic event 1b in the North Atlantic. *Sedimentology* **2011**, *58*, 1217–1246. [[CrossRef](#)]
2. McAnena, A.; Flögel, S.; Hofmann, P.; Herrle, J.O.; Griesand, A.; Pross, J.; Talbot, H.M.; Rethemeyer, J.; Wallmann, K.; Wagner, T. Atlantic cooling associated with a marine biotic crisis during the mid-Cretaceous period. *Nat. Geosci.* **2013**, *6*, 558–561. [[CrossRef](#)]
3. Sabatino, N.; Coccioni, R.; Manta, D.S.; Baudin, F.; Vallefucio, M.; Traina, A.; Sprovieri, M. High resolution chemostratigraphy of the late Aptian—Early Albian oceanic anoxic event (OAE 1b) from the Poggio le Guaine section (Umbria e Marche Basin, central Italy). *Palaeogeogr. Palaeoclimatol. Palaeoecol.* **2015**, *426*, 319–333. [[CrossRef](#)]
4. Dummann, W.; Steinig, S.; Hofmann, P.; Flögel, S.; Osborne, A.H.; Frank, M.; Herrle, J.; Bretschneider, L.; Sheward, R.; Wagner, T. The impact of Early Cretaceous gateway evolution on ocean circulation and organic carbon burial in the emerging South Atlantic and Southern Ocean basins. *Earth Planet. Sci. Lett.* **2020**, *530*, 115890. [[CrossRef](#)]
5. Castro, J.M.; de Gea, G.A.; Ruiz-Ortiz, P.A.; Nieto, L.M. Development of carbonate platforms on an extensional (rifted) margin: The Valanginian-Albian record of the Prebetic of Alicante (SE Spain). *Cretac. Res.* **2008**, *29*, 848–860. [[CrossRef](#)]

6. Ruiz-Ortiz, P.A.; Castro, J.M.; Arias, C.; Vilas, L.; Martín-Chivelet, J.; de Gea, G.A.; Molina, J.M.; Nieto, L.M.; Reolid, M.; Aguado, R.; et al. The South Iberian Continental Margin. In *The Geology of Iberia: A Geodynamic Approach, Regional Geology Reviews*; Quesada, C., Oliveira, J.T., Eds.; Springer: Cham, Switzerland, 2019; pp. 190–205. [[CrossRef](#)]
7. Frizon de Lamotte, D.; Raulin, C.; Mouchot, N.; Wrobel-Daveau, J.-C.; Blanpied, C.; Ringenbach, J.-C. The southernmost margin of the Tethys realm during the Mesozoic and Cenozoic: Initial geometry and timing of the inversion processes. *Tectonics* **2011**, *30*, TC3002. [[CrossRef](#)]
8. Chumakov, N.M.; Zharkov, M.A.; Herman, A.B.; Doludenkho, M.P.; Kalandadze, N.N.; Lebedev, E.A.; Ponomarenko, A.G.; Rautian, A.S. Climate belts of the Mid-Cretaceous time. *Stratigr. Geol. Correl.* **1995**, *3*, 241–260.
9. Hay, W.W.; Floegel, S. New thoughts about the Cretaceous climate and oceans. *Earth Sci. Rev.* **2012**, *115*, 262–272. [[CrossRef](#)]
10. Weissert, H.; Lini, A.; Föllmi, K.B.; Kuhn, O. Correlation of Early Cretaceous carbon isotope stratigraphy and platform drowning events: A possible link? *Palaeogeogr. Palaeoclimatol. Palaeoecol.* **1998**, *137*, 189–203. [[CrossRef](#)]
11. Föllmi, K.B. Early Cretaceous life, climate and anoxia. *Cretac. Res.* **2012**, *35*, 230–257. [[CrossRef](#)]
12. Frau, C.; Tendil, A.J.-B.; Pohl, A.; Lanteaume, C. Revising the timing and causes of the Urgonian rudistid-platform demise in the Mediterranean Tethys. *Glob. Planet. Change* **2020**, *187*, 103124. [[CrossRef](#)]
13. Bréhéret, J.G. The mid-Cretaceous organic-rich sediments from the Vocontian Zone of the French Southeast Basin. In *Hydrocarbon and Petroleum Geology of France*; Mascle, A., Ed.; Springer: Berlin/Heidelberg, Germany, 1994; pp. 295–320.
14. Vilas, L.; Arias, C.; Castro, J.M.; Company, M.; García-Hernández, M.; de Gea, G.A.; Ruiz-Ortiz, P.A. Ciclo IV. In *Geología de España*; Vera, J.A., Ed.; SGE-IGME: Madrid, Spain, 2004; pp. 368–369.
15. de Gea, G.A.; Castro, J.M.; Aguado, R.; Ruiz Ortiz, P.A.; Company, M. Lower Aptian carbon-isotope stratigraphy from a distal carbonate shelf setting: The Cau section, Prebetic Zone, SE Spain. *Palaeogeogr. Palaeoclimatol. Palaeoecol.* **2003**, *200*, 207–219. [[CrossRef](#)]
16. de Gea, G.A. Bioestratigrafía y Eventos del Cretácico Inferior en las Zonas Externas de la Cordillera Bética. Ph.D. Thesis, Universidad de Jaén, Jaén, Spain, 2004.
17. Castro, J.M. Las Plataformas del Valanginiense Superior-Albiense Superior en el Prebético de Alicante. Ph.D. Thesis, Universidad de Granada, Granada, Spain, 1998.
18. Skelton, P.W.; Castro, J.M.; Ruiz-Ortiz, P.A. Aptian carbonate platform development in the Southern Iberian Palaeomargin (Prebetic of Alicante, SE Spain). *BSGF-Earth Sci. Bull.* **2019**, *190*, 3. [[CrossRef](#)]
19. Vera, J.A. (Ed.) *Geología de España*; SGE-IGME: Madrid, Spain, 2004; p. 890.
20. Nieto, L.M.; Molina, J.M.; Ruiz-Ortiz, P.A.; Castro, J.M.; de Gea, G.A. Ciclos de somerización en un lagoon de baja energía (Aptiense de la Sierra de Jódar, Prebético de Jaén. Cordillera Bética). *Geotemas* **2012**, *13*, 83–87.
21. Ruiz-Ortiz, P.A.; de Gea, G.A.; Castro, J.M.; García-García, F.; Molina, J.M.; Nieto, L.M. Datos y reflexiones para la reconstrucción paleogeográfica de un sector centro-septentrional (entre Bedmar y Jaén) de la Cordillera Bética durante el Cretácico Inferior. *Rev. Soc. Geol. España.* **2014**, *27*, 111–126.
22. Molina, J.M.; Nieto, L.M.; Ruiz-Ortiz, P.A.; Castro, J.M.; de Gea, G.A. El Cretácico Inferior de la Sierra de Jódar-Bedmar (Prebético de Jaén, Cordillera Bética): Facies, bioestratigrafía e interpretación paleoambiental. *Geogaceta* **2012**, *52*, 73–76.
23. Sanz de Galdeano, C.; García-Tortosa, F.J.; Peláez, J.A. Estructura del Prebético de Jaén (sector de Bedmar). Su relación con el avance del Subbético y con fallas en el basamento. *Rev. Soc. Geol. España.* **2013**, *26*, 55–68.
24. Molina, J.M.; Nieto, L.M.; Ruiz-Ortiz, P.A.; Castro, J.M.; de Gea, G.A. Secuencias deposicionales marinas someras con estromatopóridos (Aptiense inferior, Prebético, Sierra de Bedmar-Jódar). *Geogaceta* **2015**, *57*, 79–82.
25. Gale, A.S.; Mutterlose, J.; Batenburg, S.; Gradstein, F.M.; Agterberg, F.P.; Ogg, J.G.; Petrizzo, M.R. The Cretaceous period. In *Geologic Time Scale 2020*; Gradstein, F.M., Ogg, J.G., Schmitz, M.D., Ogg, G.M., Eds.; Elsevier: Amsterdam, The Netherlands, 2020; Volume 2, pp. 1023–1086.
26. Hardenbol, J.; Thierry, J.; Farley, M.B.; Jacquin, T.; de Graciansky, P.-C.; Vail, P.R. Mesozoic and Cenozoic sequence chronostratigraphic framework of European Basins. In *Mesozoic and Cenozoic Sequence Stratigraphy of European Basins*; de Graciansky, P.-C., Hardenbol, J., Jacquin, T., Vail, P.R., Eds.; SEPM: Broken Arrow, OK, USA, 1998; Volume 60, pp. 3–13.
27. Coplen, T.B.; Brand, W.A.; Ghore, M.; Gröning, M.; Meijer, H.A.; Toman, B.; Verkouteren, R.M. New guidelines for $\delta^{13}\text{C}$ measurements. *Anal. Chem.* **2006**, *78*, 2439–2441. [[CrossRef](#)] [[PubMed](#)]
28. Castro, J.M.; Company, M.; de Gea, G.A.; Aguado, R. Biostratigraphy of the Aptian-Middle Cenomanian platform to basin domain in the Prebetic Zone of Alicante, SE Spain: Calibration between shallow water benthic and pelagic scales. *Creat. Res.* **2001**, *22*, 145–156. [[CrossRef](#)]
29. Martín-Closas, C.; Wang, Q. Historical biogeography of the lineage *Atopochara trivoltis* PECK 1941 (Cretaceous Charophyta). *Palaeogeogr. Palaeoclimatol. Palaeoecol.* **2008**, *260*, 435–451. [[CrossRef](#)]
30. Martín-Closas, C. Cosmopolitanism in Northern Hemisphere Cretaceous Charophyta (Clavatoroidae). *Palaeogeogr. Palaeoclimatol. Palaeoecol.* **2015**, *438*, 9–23. [[CrossRef](#)]
31. Lohmann, K.C. Geochemical patterns of meteoric diagenetic systems and their application to studies of paleokarst. In *Paleokarst*; James, N.P., Choquette, P.W., Eds.; Springer: New York, NY, USA, 1988; pp. 58–80.
32. Weissert, H.; Bréhéret, J.G. A carbonate-isotope record from Aptian-Albian sediments of the Vocontian trough (SE France). *Bull. Soc. Géol. France.* **1991**, *162*, 1133–1140.

33. Grötsch, J.; Billing, I.; Vahrenkamp, V. Carbon-isotope stratigraphy in shallow-water carbonates: Implications for Cretaceous black-shale deposition. *Sedimentology* **1998**, *45*, 623–634. [[CrossRef](#)]
34. Castro, J.M.; Ruiz-Ortiz, P.A.; de Gea, G.A.; Aguado, R.; Jarvis, I.; Weissert, H.; Molina, J.M.; Nieto, L.M.; Pancost, R.D.; Quijano, M.L.; et al. High-Resolution C-isotope, TOC and Biostratigraphic Records of OAE1a (Aptian) from an Expanded Hemipelagic Cored Succession, Western Tethys: A New Stratigraphic Reference for Global Correlation and Palaeoenvironmental Reconstruction. *Paleoceanogr. Paleoclimatol.* **2021**, *36*, 3. [[CrossRef](#)]
35. Wagner, T.; Wallmann, K.; Herrle, J.; Hofmann, P.; Stuesser, I. Consequences of moderate ~25,000 yr lasting emission of light CO₂ into the mid-Cretaceous ocean. *Earth Planet. Sci. Lett.* **2007**, *259*, 200–211. [[CrossRef](#)]
36. Peybernes, C.; Giraud, F.; Jaillard, E.; Robert, E.; Masrour, M.; Aoutem, M.; Içame, N. Stratigraphic framework and calcareous nannofossil productivity of the Essaouira-Agadir Basin (Morocco) during the Aptian-Early Albian: Comparison with the north-Tethyan margin. *Cretac. Res.* **2013**, *39*, 149–169. [[CrossRef](#)]
37. Basilone, L. Synsedimentary tectonics vs paleoclimatic changes across the Aptian-Albian boundary along the Southern Tethyan margin: The panormide carbonate platform case history (NW Sicily). *Mar. Pet. Geol.* **2021**, *124*, 104801. [[CrossRef](#)]
38. Capitanio, F.A.; Faccenna, C.; Funicello, R. The opening of the Sirte basin: Result of slab avalanching? *Earth Planet. Sci. Lett.* **2009**, *285*, 210–216. [[CrossRef](#)]
39. Vitale, S.; Amore, O.F.; Ciarcia, S.; Fedele, L.; Grifa, C.; Prinzi, E.P.; Tavani, S.; Tramparulo, F. Structural, stratigraphic, and petrological clues for a Cretaceous-Paleogene abortive rift in the southern Adria domain (southern Apennines, Italy). *Geol. J.* **2018**, *53*, 660–681. [[CrossRef](#)]
40. Randazzo, V.; Di Stefano, P.; Todaro, S.; Cacciatore, M.S. A Cretaceous carbonate escarpment from Western Sicily (Italy): Biostratigraphy and tectono-sedimentary evolution. *Cretac. Res.* **2020**, *110*, 104423. [[CrossRef](#)]
41. García-Hernández, M.; Castro, J.M.; Nieto, L.M. La transgresión Aptiense en la Sierra de Segura (Zona Prebética, provincia de Jaén). *Geogaceta* **2003**, *33*, 127–129.
42. Ruiz-Ortiz, P.A.; Reolid, M.; Martín-Closas, C.; Nieto, L.M.; Molina, J.M.; Castro, J.M.; Abad, I. Fossil assemblages from palustrine sediments and paleosols interfingering with shallow marine platform carbonates recorded in the Aptian-Albian transition (Prebetic, Southern Spain). In Proceedings of the XXXI Jornadas de Paleontología, Baeza, Spain, 7–10 October 2015; pp. 270–271.
43. Strasser, A.; Pittet, B.; Hillgärtner, H.; Pasquier, J.-B. Depositional sequences in shallow carbonate-dominated sedimentary systems: Concepts for high-resolution analysis. *Sediment. Geol.* **1999**, *128*, 201–221. [[CrossRef](#)]
44. Valero, L.; Huerta, P.; Garcés, M.; Armenteros, I.; Beamud, E.; Gómez-Paccard, M. Linking sedimentation rates and large-scale architecture for facies prediction in nonmarine basins (Paleogene, Almazan Basin, Spain). *Basin Res.* **2017**, *29*, 213–232. [[CrossRef](#)]
45. Herrle, J.O.; Kosler, P.; Friedrich, O.; Erlenkeuser, H.; Hemleben, C. High-resolution carbon isotope records of the Aptian to Lower Albian from SE France and the Mazagan Plateau (DSDP site 545): A stratigraphic tool for paleoceanographic and paleobiologic reconstruction. *Earth Planet. Sci. Lett.* **2004**, *218*, 149–161. [[CrossRef](#)]
46. Kennedy, W.J.; Gale, A.S.; Huber, B.T.; Petrizzo, M.R.; Bown, P.; Barchetta, A.; Jenkyns, H.C. Integrated stratigraphy across the Aptian/Albian boundary at Col de pré-Guittard (southeast France): A candidate Global Boundary Stratotype Section. *Cretac. Res.* **2014**, *51*, 248–259. [[CrossRef](#)]
47. Tsikos, H.; Karakitsios, V.; van Breugel, Y.; Walsworth-Bell, B.; Bombardiere, L.; Petrizzo, M.R.; Damsté, J.S.S.; Schouten, S.; Erba, E.; Premoli-Silva, I.; et al. Organic-carbon deposition in the Cretaceous of the Ionian Basin, NW Greece: The Paquier Event (OAE 1b) revisited. *Geol. Mag.* **2004**, *141*, 401–416. [[CrossRef](#)]
48. García-Hernández, M. El Jurásico Terminal y el Cretácico Inferior en las Sierras de Cazorla y del Segura (Zona Prebética). Ph.D. Thesis, Universidad de Granada, Granada, Spain, 1978.
49. García-Hernández, M.; Castro, J.M.; Nieto, L.M. Los carbonatos del Cretácico Inferior del Prebético de la Sierra de Segura. In *Itinerarios Geológicos por el Mesozoico de la Provincia de Jaén*; Ruiz-Ortiz, P.A., Molina, J.M., Nieto, L.M., Castro, J.M., de Gea, G.A., Eds.; Universidad de Jaén: Jaén, Spain, 2001; pp. 63–91.
50. Jenkyns, H.C. Geochemistry of oceanic anoxic events. *Geochem. Geophys. Geosyst.* **2010**, *11*, Q03004. [[CrossRef](#)]
51. Erbacher, J.; Huber, B.T.; Norris, R.D.; Markey, M. Increased thermohaline stratification as a possible cause for an ocean anoxic event in the Cretaceous period. *Nature* **2001**, *409*, 325–327. [[CrossRef](#)]
52. Robinson, S.A.; Williams, T.; Bown, P.R. Fluctuations in biosiliceous production and the generation of Early Cretaceous oceanic anoxic events in the Pacific Ocean (Shatsky Rise, Ocean Drilling Program Leg 198). *Paleoceanography* **2004**, *19*, PA4024. [[CrossRef](#)]
53. Basilone, L.; Perri, F.; Sulli, A.; Critelli, S. Paleoclimate and extensional tectonics of short-lived lacustrine environments. Lower Cretaceous of the Panormide Southern Tethyan carbonate platform (NW Sicily). *Mar. Pet. Geol.* **2017**, *88*, 428–439. [[CrossRef](#)]
54. Mutterlose, J.; Pauly, S.; Steuber, T. Temperature controlled deposition of early Cretaceous (Barremian–early Aptian) black shales in an epicontinental sea. *Palaeogeogr. Palaeoclimatol. Palaeoecol.* **2009**, *273*, 330–345. [[CrossRef](#)]
55. Charbonnier, G.; Adatte, T.; Spangenberg, J.E.; Föllmi, K.B. The expression of early Aptian to latest Cenomanian oceanic anoxic events in the sedimentary record of the Briançonnais domain. *Glob. Planet. Change* **2018**, *170*, 76–92. [[CrossRef](#)]
56. Bottini, C.; Erba, E. Mid-Cretaceous paleoenvironmental changes in the western Tethys. *Clim. Past* **2018**, *14*, 1147–1163. [[CrossRef](#)]
57. Haq, B.U. Cretaceous eustasy revisited. *Glob. Planet. Change* **2014**, *113*, 44–58. [[CrossRef](#)]
58. Friedrich, O.; Reichelt, K.; Herrle, J.O.; Lehmann, J.; Pross, J.; Hemleben, C. Formation of the Late Aptian Niveau Fallot black shales in the Vocontian Basin (SE France): Evidence from foraminifera, palynomorphs, and stable isotopes. *Mar. Micropaleontol.* **2003**, *49*, 65–85. [[CrossRef](#)]

-
59. Browning, E.L.; Watkins, D.K. Elevated primary productivity of calcareous nannoplankton associated with ocean anoxic event 1b during the Aptian/Albian transition (Early Cretaceous). *Paleoceanography* **2008**, *23*, PA2213. [[CrossRef](#)]
 60. Scotese, C.R.; Song, H.; Mills, B.J.W.; van der Meer, D.J. Phanerozoic paleotemperatures: The earth's changing climate during the last 540 million years. *Earth Sci. Rev.* **2021**, *215*, 103503. [[CrossRef](#)]